

Hidden one-dimensional, strongly nested, and almost half-filled Fermi surface in $\text{Ba}_2\text{CuO}_{3+y}$ superconductors

Paul Worm¹,[✉] Motoharu Kitatani²,[✉] Jan M. Tomczak¹,[✉] Liang Si^{1,3,*}, and Karsten Held¹

¹*Institute of Solid State Physics, TU Wien, 1040 Vienna, Austria*

²*RIKEN Center for Emergent Matter Science (CEMS), Wako, Saitama, 351-0198, Japan*

³*School of Physics, Northwest University, Xi'an 710069, China*

 (Received 25 July 2021; revised 17 November 2021; accepted 20 January 2022; published 7 February 2022)

All previous cuprate superconductors display a set of common features: (i) vicinity to a $\text{Cu } 3d^9$ configuration; (ii) separated CuO_2 planes; and (iii) superconductivity for doping $\delta \sim 0.1$ – 0.3 . Recently, Li *et al.* [*Proc. Natl. Acad. Sci. USA* **116**, 12156 (2019)] challenged this picture by discovering “highly overdoped” superconducting $\text{Ba}_2\text{CuO}_{3+y}$. Using density-functional theory plus dynamical mean-field theory, we reveal a bilayer structure of $\text{Ba}_2\text{CuO}_{3.2}$ of alternating quasi-two-dimensional (2D) and quasi-one-dimensional (1D) character. Correlations tune an interlayer self-doping leading to an almost half-filled, strongly nested, quasi-1D $d_{x^2-y^2}$ band, which is prone to strong antiferromagnetic fluctuations, possibly at the origin of superconductivity in $\text{Ba}_2\text{CuO}_{3+y}$.

DOI: [10.1103/PhysRevB.105.085110](https://doi.org/10.1103/PhysRevB.105.085110)

I. INTRODUCTION

Even 35 years after the discovery of high-temperature superconductivity in cuprates [1], the pairing mechanism remains highly controversial. In this respect, the recently discovered cuprate $\text{Ba}_2\text{CuO}_{3.2}$ [2] is supremely exciting as it puts into question common wisdom for cuprate high-temperature superconductivity. The oxygen reduction from Ba_2CuO_4 to polycrystalline $\text{Ba}_2\text{CuO}_{3+y}$ was achieved by synthesizing the samples at extremely high pressures (~ 18 GPa) and high temperatures ($\sim 1000^\circ\text{C}$). First, it is unusual that the hole concentration in the superconducting $y \sim 0.2$ phase has $\delta = 2y = 0.4$ holes with respect to a $\text{Cu } 3d^9$ electronic configuration. This is twice as many holes as in other superconducting cuprates. Despite this unusual doping the critical temperature $T_c = 70$ K is high [2].

Second, a La_2CuO_4 -type structure with space group $I4/mmm$ was suggested by the authors of Ref. [2], with a compressed oxygen octahedron, contrary to an elongated one. This compression also pushes the $3z^2 - r^2$ orbital, that is fully occupied in other cuprates, up in energy. More recent experiments [3] report, however, x-ray absorption (XAS) and resonant inelastic x-ray scattering (RIXS) data, incompatible with the La_2CuO_4 structure. These results [3] require two inequivalent Cu sites, proposing a bilayer structure. Unfortunately, single crystals have not yet been synthesized. This leaves quite an uncertainty even for the crystal structure and different ones have been suggested [2–8].

Guided by the experimental results and previous density-functional theory (DFT) calculations [4], we investigate the electronic structure of the three crystal structures of Fig. 1: the parent compound Ba_2CuO_4 [Fig. 1(a)], the fully reduced material Ba_2CuO_3 [Fig. 1(b)], and a bilayer structure $\text{Ba}_2\text{CuO}_{3.25}$

[Fig. 1(c)]. The last structure has an oxygen deficiency (excess) of 0.75 ($y = 0.25$) compared to the structure of Fig. 1(a) [Fig. 1(b)]. It is close to $y = 0.2$ but can be realized in a smaller $2 \times 2 \times 1$ unit cell by removing three oxygens (adding one oxygen). To find the ground state structure of $\text{Ba}_2\text{CuO}_{3+y}$ near $y = 0.2$, we consider all variations proposed in previous studies [4,8] and find the bilayer structure of Fig. 1(c) to be the energetically most favorable among all possible $2 \times 2 \times 1$ supercells with eight Cu sites [9].

The primitive cell [Fig. 1(c)] can be obtained from Ba_2CuO_3 [Fig. 1(b)] by inserting one oxygen into the empty spaces in the “layer 1” CuO_2 planes at the Cu-1 sites. This yields a $\text{Ba}_8\text{Cu}_4\text{O}_{13}$ supercell that contains four Cu sites, resulting in the chemical formula $\text{Ba}_2\text{CuO}_{3.25}$. It is composed of two different layers: In layer 1 we have Cu-1 sites with a sixfold octahedral CuO_6 coordination, and Cu-2 sites with planar CuO_4 squares. In layer 2 both Cu-3 and Cu-4 sites are equivalent and the same as in Ba_2CuO_3 [Fig. 1(b)] with planar CuO_4 squares. They form one-dimensional (1D) CuO chains in the b direction. If we compare to the parent compound Ba_2CuO_4 , oxygen reduction has removed the planar O in the a direction for Cu-2, Cu-3, and Cu-4 sites. Please note that removing parts of the oxygen atoms from the CuO_2 planes and forming 1D CuO chains will result in an orthorhombic distortion of $\text{Ba}_2\text{CuO}_{3.2}$, if all CuO chains point in the same direction, as discussed previously for Ba_2CuO_3 [10]. However, the synthesizing process of oxygen reduced $\text{Ba}_2\text{CuO}_{3+y}$ under high temperature and high pressure might stabilize an undistorted crystal where the CuO chains in different layers point in alternating directions. The structure is further stabilized by the fact that every other layer still contains a - b symmetric CuO_6 octahedra.

In this paper, we present DFT and DFT+dynamical mean-field theory (DMFT) [11–13] calculations for all three crystal structures of Fig. 1 as well as for the superconducting $\text{Ba}_2\text{CuO}_{3.2}$. To obtain the hole doping of the latter, we employ

*liang.si@ifp.tuwien.ac.at

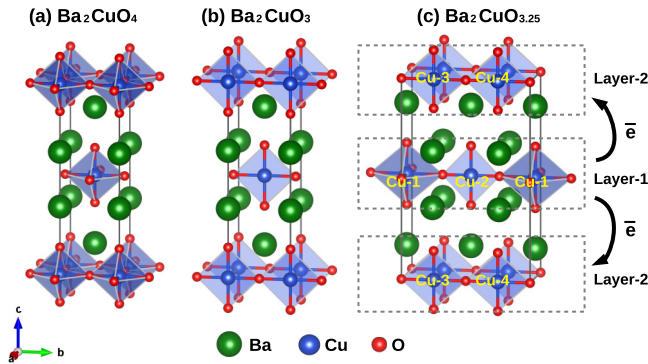


FIG. 1. Crystal structure of (a) the parent compound Ba_2CuO_4 and (b) the ideal, fully reduced Ba_2CuO_3 , where the planar oxygen atoms in the a direction are vacant. (c) Energetically favorable crystal structure for $\text{Ba}_2\text{CuO}_{3.25}$ [4] close to the superconducting doping $y = 0.2$. Note (c) forms a bilayer structure, layer 2 has as (b) the in-plane oxygens in the a direction removed, and in layer 1 every second one is removed. This leads in layer 2 to 1D $\text{Cu-3-O-Cu-4-O}\dots$ chains. Arrows indicate the interlayer charge transfer that is driven by electronic correlations.

a rigid (band-structure) doping. We find that the physics is completely different for the three structures: Ba_2CuO_4 is a two-orbital system, while Ba_2CuO_3 is a one-orbital 1D system. The $\text{Ba}_2\text{CuO}_{3.25}$ supercell inherits aspects of both parent compounds in its two inequivalent layers. Crucially, correlations induce a charge transfer so that layer 2 of $\text{Ba}_2\text{CuO}_{3.25}$ is doped close to half filling and thus prone to strong antiferromagnetic spin fluctuations.

II. METHODS

DFT-level computations are performed by WIEN2K [14,15] using the Perdew-Burke-Ernzerhof [16] version of the generalized gradient approximation (GGA-PBE) on a dense momentum grid with 2000 k points totally. The structural parameters of ideal Ba_2CuO_4 and Ba_2CuO_3 are adopted from Refs. [2,17], and the crystal structure of the bilayer $\text{Ba}_2\text{CuO}_{3.25}$ phase was optimized within DFT-PBE (see Supplemental Material [18] for details on computation and other structures, including Refs. [19–27]). As an input for the DMFT calculations a low-energy effective Hamiltonian is generated by projecting the WIEN2K bands around the Fermi level onto Wannier functions [28,29] using WIEN2WANNIER [30,31]. These are supplemented by a local Kanamori interaction and the fully localized limit as double counting [32]. Constrained random phase approximation (cRPA) [33] calculations motivate an intraorbital Hubbard interaction $U = 2.6$ eV and a Hund's exchange $J = 0.3$ eV (see Supplemental Material [18]). For the interorbital interaction we use $U' = U - 2J$. In our calculations we used slightly enhanced Hubbard interactions $U = 3.0$ eV to mimic the disregarded frequency dependence of U , along the lines of Ref. [34] and many other publications [35]. We solve the resulting many-body Hamiltonian at room temperature (300 K) within DMFT employing a continuous-time quantum Monte Carlo solver in the hybridization expansions [36] using w2DYNAMICS [37,38]. Real-frequency spectra are obtained

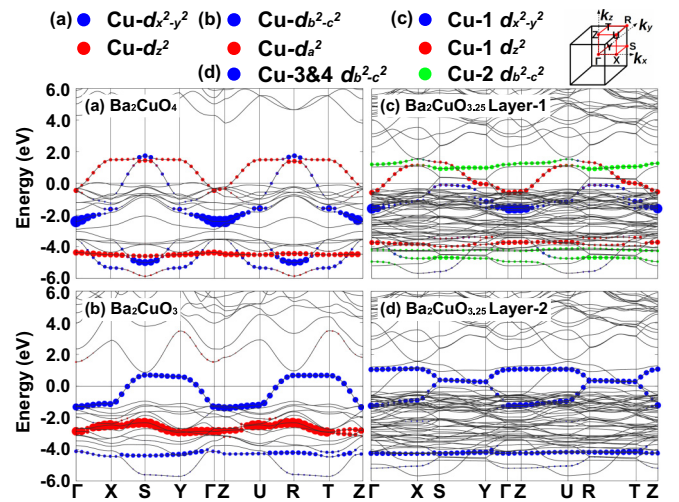


FIG. 2. DFT band structure and orbital character for (a) Ba_2CuO_4 , (b) Ba_2CuO_3 , (c) $\text{Ba}_2\text{CuO}_{3.25}$ layer 1, and (d) $\text{Ba}_2\text{CuO}_{3.25}$ layer 2 along a high-symmetry path through the Brillouin zone (see top right).

with the ANA_CONT code [39] via analytic continuation using the maximum entropy method (MaxEnt).

III. RESULTS

A. DFT electronic structure

Let us first review the DFT electronic structure for the three different crystal structures. For Ba_2CuO_4 the Fermi surface (FS) in Fig. 2(a) is composed of two Cu- d bands of $d_{x^2-y^2}$ and d_{z^2} orbital character, consistent with previous results [2,40] and hinting toward multiorbital physics. Instead, Ba_2CuO_3 in Fig. 2(b) hosts only one Fermi surface sheet of $d_{b^2-c^2}$ orbital character [4] (this orbital is as an $x^2 - y^2$ orbital only in the bc plane as the missing oxygen in the a direction dictates the local symmetry). Because the Cu layers are well separated in the c direction, this leads to a quasi-1D character of the band structure in the b direction. Superconductivity was, however, observed in neither of these two parent compounds, but at an oxygen concentration $y = 0.2$ for $\text{Ba}_2\text{CuO}_{3.2}$. A rigid band shift of the Ba_2CuO_3 or Ba_2CuO_4 band structure to this $y = 0.2$ doping results in two profoundly different FSs (see Figs. 3 and 5 below), electronic structures, and even orbital occupations. This naturally prompts the following question: Does the FS of $\text{Ba}_2\text{CuO}_{3.2}$ show Ba_2CuO_3 or Ba_2CuO_4 character? To address this question, we perform a supercell calculation, which allows for nonuniform oxygen reduction [4]. We identify the most promising structure for $\text{Ba}_2\text{CuO}_{3.25}$ (which is reasonably close to one of the experimental oxygen concentrations) to be the one in Fig. 1(c), based on the DFT total energy (see Supplemental Material Sec. 1 [18]). This structure has two inequivalent layers, each of which is similar to the two parent compounds: The Cu-1 sites in layer 1 have the same local octahedra as in Ba_2CuO_4 , and its low-energy excitations in Fig. 2(c) are hence similarly described by a Cu- $d_{x^2-y^2}$ and a Cu- d_{z^2} orbital. The Cu-2 site in layer 1 has an oxygen removed and hosts a $d_{b^2-c^2}$ band, which does not cross the Fermi level in Fig. 2(c). The Cu-3 and Cu-4 sites in layer

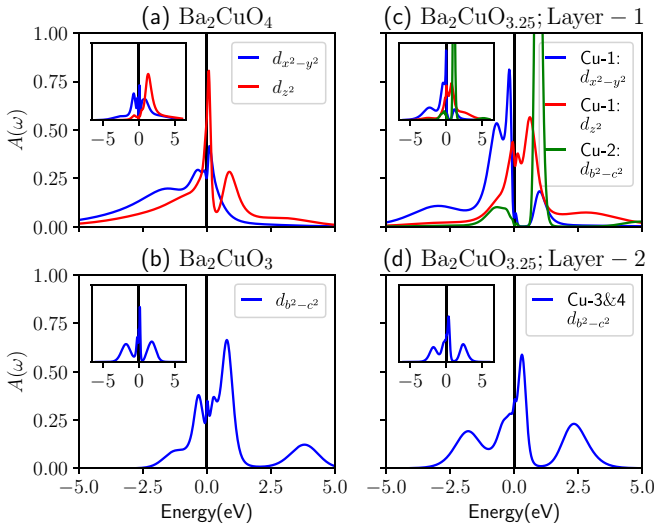


FIG. 3. DMFT spectral function $A(\omega)$ using the Wannier-projected low-energy bands of Fig. 2 for the three crystal structures: (a) Ba_2CuO_4 , (b) Ba_2CuO_3 , (c) $\text{Ba}_2\text{CuO}_{3.25}$ layer 1, and (d) $\text{Ba}_2\text{CuO}_{3.25}$ layer 2. The inset shows results for the stoichiometric parent compound, and the main panel corresponds to the hole doping of $\text{Ba}_2\text{CuO}_{3.2}$. The insets have the same scale as the main panels.

2, on the other hand, display the same local surroundings as Ba_2CuO_3 and their low-energy electronic structure as in Fig. 2(d) is described by a single $d_{b^2-c^2}$ orbital [41,42]. This band is similar to Fig. 2(b) (see also the hopping elements in Table I).

B. DFT + DMFT electronic structure

Since cuprates are known for strong correlation effects, we expect significant corrections to the DFT results. To address these we perform DFT + DMFT calculations in the paramagnetic phase at room temperature (300 K). The DMFT momentum-integrated spectral function $A(\omega)$ is displayed in Fig. 3. We show the spectrum both for the stoichiometric parent compound (inset) and an adjusted particle number (main panel) to reach an oxygen concentration of $y = 0.2$. The arguably simplest system is undoped Ba_2CuO_3 [Fig. 3(b) inset] which shows a single low-energy orbital with the typical three-peak spectrum of correlated electron systems. Besides a lower and an upper Hubbard band, there is a central quasi-particle peak with mass enhancement $m^*/m \equiv 1/Z \sim 3.85$. Please note that we are considering the paramagnetic solution, even though without doping Ba_2CuO_3 has a strong tendency to antiferromagnetism [4]. Upon doping [see Fig. 3(b)], corre-

TABLE I. Major hopping elements in meV for the $d_{b^2-c^2}$ orbital in Ba_2CuO_3 and layer 2 of $\text{Ba}_2\text{CuO}_{3.25}$. t_{abc} indicates the hopping along the real-space vector R_{abc} , and a, b, c are the number of unit cells along the x, y , and z direction.

Structure	t_{100}	t_{200}	t_{010}	t_{020}	t_{110}
Ba_2CuO_3	-18.5	-1.3	-470.2	-84.6	-6.8
$\text{Ba}_2\text{CuO}_{3.25}$	-25.8	1.4	-518.1	-89.4	-11.9

lation effects become much weaker as evidenced by a reduced mass enhancement of $m^*/m \sim 1.45$. The other parent compound, Ba_2CuO_4 in Fig. 3(a), hosts two orbitals: a moderately correlated $d_{x^2-y^2}$ orbital close to half filling [(spin-summed) occupation $n \sim 0.87$, $m^*/m \sim 1.39$] and a weakly correlated d_{z^2} orbital ($n \sim 0.13$, $m^*/m \sim 1.15$). A metallic behavior at this doping was also reported previously in Ref. [43]. Removing $1 - y = 0.8$ oxygen per formula, electrons dope both orbitals, and slightly increase the mass enhancement in the $d_{x^2-y^2}$ orbital ($n \sim 1.56$, $m^*/m \sim 1.47$) while dramatically boosting it for the d_{z^2} orbital ($n \sim 1.04$, $m^*/m \sim 3.12$).

We now assess how these trends survive in the structurally similar Cu-O planes of the bilayer compound $\text{Ba}_2\text{CuO}_{3.25}$. Let us thus turn to Figs. 3(c) and 3(d) which show layer 1 and layer 2 spectra of the bilayer structure $\text{Ba}_2\text{CuO}_{3.25}$, respectively. Here, correlations play a crucial role: They drive a charge transfer from layer 1 to layer 2. As a consequence, the occupation of the $d_{b^2-c^2}$ orbital in layer 2 is increased towards half filling ($n \sim 0.91$). This leads to a strongly correlated spectrum in Fig. 3(d) with $m^*/m \sim 2.40$. For Ba_2CuO_3 , we would have a similar $m^*/m \sim 2.63$, if the occupation is fixed at 0.9 electrons per $d_{b^2-c^2}$ orbital. Hence, we conclude that the strongly correlated, half-filled, single $d_{b^2-c^2}$ band physics is preserved in the $\text{Ba}_2\text{CuO}_{3.2}$ structure. As superconductivity is known to be extremely sensitive to doping [44,45], let us now discuss this important charge transfer in more detail.

IV. DISCUSSION

A. Correlation-induced charge transfer

One common ingredient for cuprate and recently observed nickelate superconductors [34,46] has been the CuO_2 or NiO_2 plane, whose low-energy physics is dominated by a $d_{x^2-y^2}$ orbital close to half filling [1,47]. Neither Ba_2CuO_3 nor Ba_2CuO_4 fits into this CuO_2 plane category. The former hosts an overdoped, quasi-1D $d_{b^2-c^2}$ band, while the latter displays two-orbital $d_{x^2-y^2}$ and d_{z^2} physics. Both compounds have been studied theoretically and several mechanisms for the superconductivity have already been proposed [6,8,40,43,48–50]. Let us stress that a rigid band-structure doping from either parent compound will always be plagued by the ambiguity of which structure is realized for the experimental $\text{Ba}_2\text{CuO}_{3.2}$ compound, especially since both parent compounds are far away from the superconducting oxygen content. This problem is resolved by turning to a supercell calculation. Here, the stabilization of a bilayer structure is crucial. However, a naive electron count for the three inequivalent Cu sites of Fig. 1(c) would be Cu-1: d^7 , Cu-2: d^9 , and Cu-3 and Cu-4: d^9 when considering the local CuO_6 and CuO_4 configurations. A charge transfer between Cu-1 and Cu-2 can be expected, as they are located in the same layer and connected by oxygen. Somewhat less straightforward but arguably more interesting is the interlayer charge transfer. In DFT, for $\text{Ba}_2\text{CuO}_{3.25}$, about ~ 0.44 electrons will relocate from layer 2 into layer 1, which results in an occupation of ~ 0.78 for the Cu-3 and Cu-4 $d_{b^2-c^2}$ orbitals.

Local DMFT correlations counteract this charge transfer. They favor an even distribution of electrons among the orbitals (see Table II). Specifically, ~ 0.12 electrons relocate back to

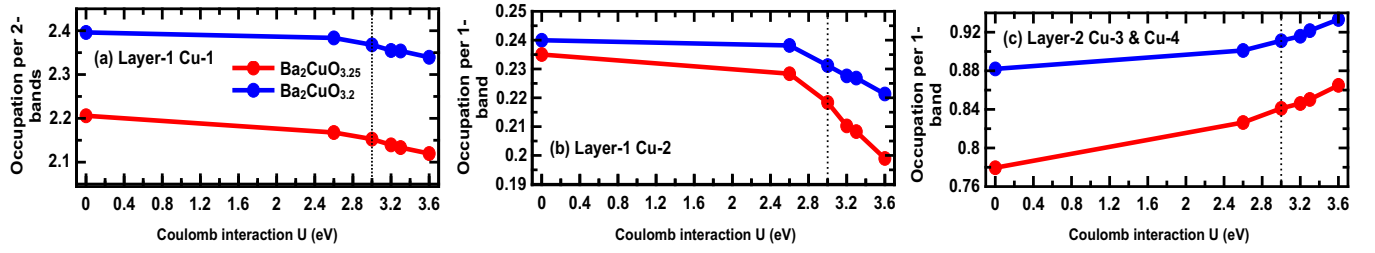


FIG. 4. DMFT calculated atom-resolved electronic occupations of the low-energy bands in $\text{Ba}_2\text{CuO}_{3.25}$. (a) Layer 1 Cu-1, (b) layer 1 Cu-2, and (c) layer 2 Cu-3 and Cu-4. Red denotes the filling of the supercell of $\text{Ba}_2\text{CuO}_{3.25}$ and blue was statically doped to match the experimentally optimized oxygen concentration of $\text{Ba}_2\text{CuO}_{3.2}$. The correlation driven charge transfer from layer 1 to layer 2 is clearly visible. Dashed lines mark $U = 3.0$ eV, which was used for the results presented in the main text.

the Cu-3 and Cu-4 sites in layer 2, leading to 0.84 electrons per $d_{b^2-c^2}$ orbital on these sites. As the oxygen content of $\text{Ba}_2\text{CuO}_{3.25}$ is already close to the experimental compound $\text{Ba}_2\text{CuO}_{3.2}$, a rigid doping to $\text{Ba}_2\text{CuO}_{3.2}$ is more justified here, and the occupations of the various orbitals are also listed in Table II. Of particular interest are the Cu-3 and Cu-4 $d_{b^2-c^2}$ orbitals in layer 2, which are now unexpectedly close to typical doping levels of common quasi-2D cuprate superconductors.

B. Dependence on the interaction value U

We used $U = 3.0$ eV as the Hubbard interaction, which represents an enhanced value of $U(\omega = 0)$ obtained by cRPA to account for the neglected frequency dependence. This enhancement is guided by the success of previous works such as Ref. [34] and many others. Nevertheless, additionally to $U = 3.0$ eV, we performed calculations for several interaction values starting with the $\omega = 0$ value of cRPA, 2.6 eV, and larger values $U = 3.2, 3.3,$ and 3.6 eV. We show the orbital occupation for the low-energy bands in the $\text{Ba}_2\text{CuO}_{3.25}$ structure as a function of this interaction strength U in Fig. 4. As

the interaction strength increases, more electrons are relocated from layer 1 [Figs. 4(a) and 4(b)] to layer 2 [Fig. 4(c)], clearly indicating that the charge transfer is driven by electronic correlations. Figure 4 further shows that the presented scenario is qualitatively stable with respect to reasonable variations in the interaction parameters.

C. FS and nesting: A connection to high T_c

With the discussion above we demonstrated that the bilayer structure of $\text{Ba}_2\text{CuO}_{3.25}$ satisfies one of the common ingredients for cuprates: Namely the low-energy physics of layer 2 is described by a single, almost half-filled orbital. However, contrary to the conventional CuO_2 planes, we have a CuO chain structure with a quasi-1D low-energy orbital, as can be seen from the FS in Fig. 5(f). Already the parent compound Ba_2CuO_3 in Fig. 5(c) has such a 1D character, but at quite a different filling. The Cu-1 FS of layer 1 in Figs. 5(d) and 5(e) has instead a two-orbital character. However, it differs from Ba_2CuO_4 in Figs. 5(a) and 5(b)—not only by the filling (volume of the FS) but also because the Cu-2 sites are insulating. The latter cuts off, among others, the hopping of the Cu-1 d_{z^2} orbital in the y direction.

Figure 5(f) shows that the correlation-induced charge transfer results not only in a $d_{b^2-c^2}$ orbital closer to half filling but also in an almost perfectly nested FS. The nesting vector of $\mathbf{k}_N \simeq \{\pi, \pi - \delta, 0\}$ is similar to the dominant vector for commensurate, antiferromagnetic fluctuations ($\mathbf{k}_{\text{AF}} = \{\pi, \pi, 0\}$), and takes through its k_x component also the slight warping of the FS into account.

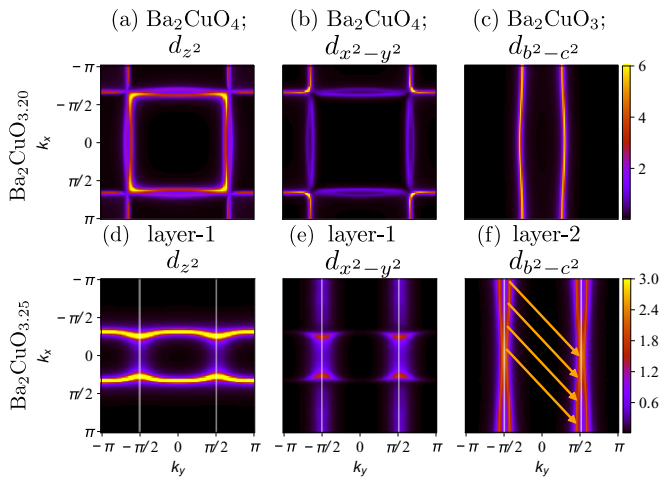


FIG. 5. DMFT FS at $k_z = 0$ for the nominal doping of $\text{Ba}_2\text{CuO}_{3.25}$ realized in the three crystal structures of Fig. 1: Ba_2CuO_4 [(a) and (b) for d_{z^2} and $d_{x^2-y^2}$], Ba_2CuO_3 (c), $\text{Ba}_2\text{CuO}_{3.25}$ layer 1 [(d) and (e) for d_{z^2} and $d_{x^2-y^2}$ of Cu-1; Cu-2 is not shown because of its tiny occupation and insulating nature], and $\text{Ba}_2\text{CuO}_{3.25}$ layer 2 (f) where we also plotted the antiferromagnetic nesting vector.

TABLE II. DFT and DMFT electron occupations for the Cu sites of $\text{Ba}_2\text{CuO}_{3.25}$ and its rigid doping to $\text{Ba}_2\text{CuO}_{3.2}$.

Site	Orbital	$\text{Ba}_2\text{CuO}_{3.25}$		$\text{Ba}_2\text{CuO}_{3.20}$	
		DFT	DMFT	DFT	DMFT
Cu-1	$d_{x^2-y^2}$	1.70	1.65	1.75	1.73
Cu-1	d_{z^2}	0.50	0.50	0.64	0.63
Cu-1	$d_{x^2-y^2} + d_{z^2}$	2.20	2.15	2.40	2.37
Cu-2	$d_{b^2-c^2}$	0.23	0.21	0.24	0.23
Cu-3 and Cu-4	$d_{b^2-c^2}$	0.78	0.84	0.88	0.91

V. CONCLUSION

High-temperature superconductivity remains one of the most puzzling phenomena in condensed matter physics and an overarching understanding is still missing. Hence, identifying common traits among superconductors, which helps us to focus on the essential ingredients, is of vital importance. The recently discovered $\text{Ba}_2\text{CuO}_{3.2}$ superconductor challenges the current picture of cuprate superconductivity. Its high hole doping concentration, compressed octahedra, and putative multiband physics baffled the scientific community. In this work, we provide a resolution to the high doping of the compound by identifying a charge transfer process, which ultimately leads to one layer hosting a single-orbital Fermi surface which is close to half filling and almost perfectly nested. This bilayer structure also resolves the ambiguity, whether a Ba_2CuO_3 or Ba_2CuO_4 structure is realized at the superconducting oxygen concentration of $\text{Ba}_2\text{CuO}_{3.2}$. Structural motives of both exist in the two layers, but the bilayer structure results in different dopings than previously thought.

Due to its strong nesting, layer 2 with its single orbital appears to be the natural candidate to host superconductivity. Layer 1, instead, serves more as a charge carrier reservoir/sink. This insight shifts the focus from a highly overdoped to a quasi-1D superconductor, which is still in contrast to all other known cuprate superconductors that are 2D. Fluctuation exchange (FLEX) calculations predict p -wave superconductivity or the pair density wave state for such an

almost perfectly nested 1D system [51]. A T_c as high as 70 K would, however, be unparalleled for a p -wave superconductor, calling for further theoretical work on such quasi-1D systems.

Hopefully, future single crystals will allow for a better crystallographic analysis, so that one can verify whether the bilayer structure is truly realized. Let us emphasize that the precise, in our case alternating, oxygen arrangement in layer 1 is of less relevance since this layer is not the one driving the system to be superconducting. Even with the ideal, ordered oxygen arrangement Cu-1 and Cu-2 have a similar $3d^{8.3}$ and $3d^{8.2}$ [52] electronic configuration, respectively, whereas the equivalent Cu-3 and Cu-4 sites in layer 2 have a distinct $3d^{8.9}$ filling. This may explain the two-peak structure of the x-ray spectrum in Ref. [3]. Last but not least, the prospects of a p -wave symmetry of the superconducting order parameter at an unprecedented high T_c calls for further experiments.

Note added. Recently, we became aware of a DFT electronic structure calculation [53] for the bilayer structure $\text{Ba}_2\text{CuO}_{3.25}$.

ACKNOWLEDGMENTS

We thank R. Arita and A. Prokofiev for helpful comments and discussions, as well as P. Kappl for proofreading the manuscript. This work was supported by the Austrian Science Fund (FWF) through Project No. P 32044, and JSPS KAKENHI Grants No. JP20K22342 and No. JP21K13887. Calculations have been done on the Vienna Scientific Cluster (VSC).

-
- [1] J. G. Bednorz and K. A. Müller, *Z. Phys. B: Condens. Matter* **64**, 189 (1986).
 - [2] W. M. Li, J. F. Zhao, L. P. Cao, Z. Hu, Q. Z. Huang, X. C. Wang, Y. Liu, G. Q. Zhao, J. Zhang, Q. Q. Liu *et al.*, *Proc. Natl. Acad. Sci. USA* **116**, 12156 (2019).
 - [3] R. Fumagalli, A. Nag, S. Agrestini, M. Garcia-Fernandez, A. C. Walters, D. Betto, N. B. Brookes, L. Braicovich, K.-J. Zhou, G. Ghiringhelli, and M. Moretti Sala, *Physica C: Supercond. Appl.* **581**, 1353810 (2021).
 - [4] K. Liu, Z.-Y. Lu, and T. Xiang, *Phys. Rev. Materials* **3**, 044802 (2019).
 - [5] Z. Wang, S. Zhou, W. Chen, and F.-C. Zhang, *Phys. Rev. B* **101**, 180509(R) (2020).
 - [6] K. Jiang, C. Le, Y. Li, S. Qin, Z. Wang, F. Zhang, and J. Hu, *Phys. Rev. B* **103**, 045108 (2021).
 - [7] Y. Li, S. Du, Z.-Y. Weng, and Z. Liu, *Phys. Rev. Materials* **4**, 044801 (2020).
 - [8] K. Yamazaki, M. Ochi, D. Ogura, K. Kuroki, H. Eisaki, S. Uchida, and H. Aoki, *Phys. Rev. Research* **2**, 033356 (2020).
 - [9] Details on lattice relaxation and a table containing all energies can be found in the Supplemental Material [18].
 - [10] H. Yamamoto, M. Naito, and H. Sato, *Physica C: Supercond.* **338**, 29 (2000).
 - [11] A. Georges, G. Kotliar, W. Krauth, and M. J. Rozenberg, *Rev. Mod. Phys.* **68**, 13 (1996).
 - [12] G. Kotliar and D. Vollhardt, *Phys. Today* **57**(3), 53 (2004).
 - [13] K. Held, *Adv. Phys.* **56**, 829 (2007).
 - [14] P. Blaha, K. Schwarz, G. Madsen, D. Kvasnicka, and J. Luitz, *WIEN2K: An Augmented Plane Wave+Local Orbitals Program for Calculating Crystal Properties* (Technische Universität Wien, Vienna, 2001).
 - [15] K. Schwarz, P. Blaha, and G. Madsen, *Comput. Phys. Commun.* **147**, 71 (2002).
 - [16] J. P. Perdew, A. Ruzsinszky, G. I. Csonka, O. A. Vydrov, G. E. Scuseria, L. A. Constantin, X. Zhou, and K. Burke, *Phys. Rev. Lett.* **100**, 136406 (2008).
 - [17] A. Khoroshilov and I. Shaplygin, *Neorgan. Mater.* **30**, 579 (1994).
 - [18] See Supplemental Material at <http://link.aps.org/supplemental/10.1103/PhysRevB.105.085110> for discussions on computational details and additional supporting results, which includes Refs. [19–27].
 - [19] G. Pizzi, V. Vitale, R. Arita, S. Blügel, F. Freimuth, G. Géranton, M. Gibertini, D. Gresch, C. Johnson, T. Koretsune, J. Ibañez-Azpiroz, H. Lee, J.-M. Lihm, D. Marchand, A. Marrazzo, Y. Mokrousov, J. I. Mustafa, Y. Nohara, Y. Nomura, L. Paulatto *et al.*, *J. Phys.: Condens. Matter* **32**, 165902 (2020).
 - [20] J. Kaufmann, P. Gunacker, A. Kowalski, G. Sangiovanni, and K. Held, *Phys. Rev. B* **100**, 075119 (2019).
 - [21] G. Kresse and J. Furthmüller, *Phys. Rev. B* **54**, 11169 (1996).
 - [22] G. Kresse and J. Hafner, *J. Phys.: Condens. Matter* **6**, 8245 (1994).

- [23] F. Aryasetiawan, M. Imada, A. Georges, G. Kotliar, S. Biermann, and A. I. Lichtenstein, *Phys. Rev. B* **70**, 195104 (2004).
- [24] T. Miyake, F. Aryasetiawan, and M. Imada, *Phys. Rev. B* **80**, 155134 (2009).
- [25] J. P. Perdew, K. Burke, and M. Ernzerhof, *Phys. Rev. Lett.* **77**, 3865 (1996).
- [26] M. Casula, A. Rubtsov, and S. Biermann, *Phys. Rev. B* **85**, 035115 (2012).
- [27] A. van Roekeghem, T. Ayril, J. M. Tomczak, M. Casula, N. Xu, H. Ding, M. Ferrero, O. Parcollet, H. Jiang, and S. Biermann, *Phys. Rev. Lett.* **113**, 266403 (2014).
- [28] G. H. Wannier, *Phys. Rev.* **52**, 191 (1937).
- [29] N. Marzari, A. A. Mostofi, J. R. Yates, I. Souza, and D. Vanderbilt, *Rev. Mod. Phys.* **84**, 1419 (2012).
- [30] A. A. Mostofi, J. R. Yates, Y.-S. Lee, I. Souza, D. Vanderbilt, and N. Marzari, *Comput. Phys. Commun.* **178**, 685 (2008).
- [31] J. Kuneš, R. Arita, P. Wissgott, A. Toschi, H. Ikeda, and K. Held, *Comput. Phys. Commun.* **181**, 1888 (2010).
- [32] V. I. Anisimov, J. Zaanen, and O. K. Andersen, *Phys. Rev. B* **44**, 943 (1991).
- [33] T. Miyake and F. Aryasetiawan, *Phys. Rev. B* **77**, 085122 (2008).
- [34] M. Kitatani, L. Si, O. Janson, R. Arita, Z. Zhong, and K. Held, *npj Quantum Mater.* **5**, 59 (2020).
- [35] While the bandwidth narrowing from $U(\omega)$ is counteracted by exchange contributions to the self-energy [54,55] that we neglect, the enhanced static U mimics the loss of low-energy spectral weight to plasmonlike satellites [56].
- [36] E. Gull, A. J. Millis, A. I. Lichtenstein, A. N. Rubtsov, M. Troyer, and P. Werner, *Rev. Mod. Phys.* **83**, 349 (2011).
- [37] N. Parragh, A. Toschi, K. Held, and G. Sangiovanni, *Phys. Rev. B* **86**, 155158 (2012).
- [38] M. Wallerberger, A. Hausoel, P. Gunacker, A. Kowalski, N. Parragh, F. Goth, K. Held, and G. Sangiovanni, *Comput. Phys. Commun.* **235**, 388 (2019).
- [39] J. Kaufmann and K. Held, [arXiv:2105.11211](https://arxiv.org/abs/2105.11211).
- [40] T. Maier, T. Berlijn, and D. J. Scalapino, *Phys. Rev. B* **99**, 224515 (2019).
- [41] J. E. Gubernatis, M. Jarrell, R. N. Silver, and D. S. Sivia, *Phys. Rev. B* **44**, 6011 (1991).
- [42] A. W. Sandvik, *Phys. Rev. B* **57**, 10287 (1998).
- [43] Y. Ni, Y.-M. Quan, J. Liu, Y. Song, and L.-J. Zou, *Phys. Rev. B* **103**, 214510 (2021).
- [44] D. Rybicki, M. Jurkutat, S. Reichardt, C. Kapusta, and J. Haase, *Nat. Commun.* **7**, 11413 (2016).
- [45] M. Qin, T. Schäfer, S. Andergassen, P. Corboz, and E. Gull, [arXiv:2104.00064](https://arxiv.org/abs/2104.00064).
- [46] D. Li, K. Lee, B. Y. Wang, M. Osada, S. Crossley, H. R. Lee, Y. Cui, Y. Hikita, and H. Y. Hwang, *Nature (London)* **572**, 624 (2019).
- [47] P. W. Anderson, *Science* **235**, 1196 (1987).
- [48] Z.-Q. Gao, K.-W. Sun, and F. Wang, *Eur. Phys. J. B* **94**, 233 (2021).
- [49] M. Klett, T. Schwemmer, S. Wolf, X. Wu, D. Riegler, A. Dittmaier, D. Di Sante, G. Li, W. Hanke, S. Rachel, and R. Thomale, *Phys. Rev. B* **104**, L100502 (2021).
- [50] M. Zegrodnik, P. Wójcik, and J. Spałek, *Phys. Rev. B* **103**, 144511 (2021).
- [51] This 1D chain is included in Refs. [57,58] as the extreme case of the anisotropic triangular lattice with hopping $t_2 = 0$.
- [52] Note that, on top of Table II, two electrons fill the the d_{z^2} of Cu-2 sites.
- [53] H.-S. Jin, W. E. Pickett, and K.-W. Lee, *Phys. Rev. B* **104**, 054516 (2021).
- [54] T. Miyake, C. Martins, R. Sakuma, and F. Aryasetiawan, *Phys. Rev. B* **87**, 115110 (2013).
- [55] J. M. Tomczak, M. Casula, T. Miyake, and S. Biermann, *Phys. Rev. B* **90**, 165138 (2014).
- [56] M. Casula, P. Werner, L. Vaugier, F. Aryasetiawan, T. Miyake, A. J. Millis, and S. Biermann, *Phys. Rev. Lett.* **109**, 126408 (2012).
- [57] K. Shigeta, S. Onari, K. Yada, and Y. Tanaka, *Phys. Rev. B* **79**, 174507 (2009).
- [58] S. Yoshida, K. Yada, and Y. Tanaka, *Phys. Rev. B* **104**, 094506 (2021).